Endothelial Cell Proteomic Response to *Rickettsia conorii* Infection Reveals Activation of the Janus Kinase (JAK)-Signal Transducer and Activator of Transcription (STAT)-Inferferon Stimulated Gene (ISG)15 Pathway and Reprogramming Plasma Membrane Integrin/Cadherin Signaling*[S]

Yingxin Zhao‡§¶, Gustavo Valbuena§‖, David H. Walker‖, Michal Gazi‖, Marylin Hidalgo, Rita DeSousa‡‡, Jose Antonio Oteo§§, Yenny Goez‖, and Allan R. Brasier‡§¶ ¶¶**

Rickettsia conorii **is the etiologic agent of Mediterranean spotted fever, a re-emerging infectious disease with significant mortality. This Gram-negative, obligately intracellular pathogen is transmitted via tick bites, resulting in disseminated vascular endothelial cell infection with vascular leakage. In the infected human, *Rickettsia conorii* infects endothelial cells, stimulating expression of cytokines and pro-coagulant factors. However, the integrated proteomic response of human endothelial cells to *R. conorii* infection is not known. In this study, we performed quantitative proteomic profiling of primary human umbilical vein endothelial cells (HUVECs) with established *R conorii* infection *versus* those stimulated with endotoxin (LPS) alone. We observed differential expression of 55 proteins in HUVEC whole cell lysates. Of these, we observed induction of signal transducer and activator of transcription (STAT)1, MX dynamin-like GTPase (MX1), and ISG15 ubiquitin-like modifier, indicating activation of the JAK-STAT signaling pathway occurs in *R. conorii*-infected HUVECs. The down-regulated proteins included those involved in the pyrimidine and arginine biosynthetic pathways. A highly specific biotinylated cross-linking enrichment protocol was performed to identify dysregulation of 11 integral plasma membrane proteins that included up-regulated expression of a sodium/potassium transporter and down-regulation of α-actin 1. Analysis of Golgi and soluble Golgi fractions identified up-regulated proteins involved in platelet-endothelial adhesion, phospholipase activity, and IFN activity. Thirty four rickettsial proteins were identified with high confidence in the Golgi, plasma membrane, or secreted protein fractions. The host proteins associated with rickettsial infections indicate activation of interferon-STAT signaling pathways; the disruption of cellular adhesion and alteration of antigen presentation pathways in response to rickettsial infections are distinct from those produced by nonspecific LPS stimulation. These patterns of differentially expressed proteins suggest mechanisms of pathogenesis as well as methods for diagnosis and monitoring *Rickettsia* infections.** ***Molecular & Cellular Proteomics 15: 10.1074/mcp.M115.054361, 289–304, 2016.***

From the Departments of ‡Internal Medicine and ‖Pathology, §Institute for Translational Sciences, and ¶Sealy Center for Molecular Medicine, University of Texas Medical Branch, Galveston, Texas 77555–1060, the **Microbiology Department, Faculty of Sciences, Pontificia Universidad Javeriana, Bogotá, Colombia, the ‡‡Centre for the Study of Vectors and Infectious Diseases Dr. Francisco Cambournac, National Institute of Health Dr. Ricardo Jorge, Águas de Moura, Av. Padre Cruz, Lisbon, 1649–016, Portugal, and the §§Centre of Rickettsiosis and Arthropod-Borne Diseases, Hospital San Pedro-Centro de Investigation Biomedical de la Rioja (CIBIR), Logroño, La Rioja, 26006, Spain

Received August 4, 2015, and in revised form, October 28, 2015
Published, MCP Papers in Press, November 11, 2015, DOI 10.1074/mcp.M115.054361

Author contributions: Y.Z., G.V., D.H.W., M.H., R.D., J.A.O., and A.R.B. designed the research; Y.Z., G.V., M.G., and Y.G. performed the research; Y.Z., G.V., M.H., R.D., and A.R.B. contributed new reagents or analytic tools; Y.Z., G.V., D.H.W., and A.R.B. analyzed the data; and Y.Z., G.V., D.H.W., J.A.O., and A.R.B. wrote the paper.

The genus *Rickettsia* contains non-motile, Gram-negative, obligately intracellular alphaproteobacteria that are of global medical and veterinary health importance due to their endemicity and re-emergence. From the clinical and antigenic perspectives, rickettsial diseases are classified into two groups, spotted fever and typhus. Nearly all of the numerous spotted fever group rickettsiae are transmitted by ticks. The

most virulent ones are *Rickettsia rickettsii*, the agent of Rocky Mountain spotted fever, and *Rickettsia conorii,* the agent of Mediterranean spotted fever (boutonneuse fever), a disease prevalent throughout the Mediterranean, Africa, the Middle East, and India. In humans, the spotted fevers present as acute fever, headache, maculopapular rash, and vascular leakage that can lead to significant morbidity and mortality due to pulmonary and cerebral edema, particularly if there are delays in diagnosis and treatment (1).

The characteristic leakage of intravascular fluid is a consequence of the specific tropism of rickettsiae for endothelial cells (1). Rickettsial organisms enter endothelial cells through a calcium-dependent zipper-like entry mechanism involving the actin cytoskeleton (2–4). Viable organisms subsequently exit the phagosomes via phospholipase D and hemolysin activities (5, 6), replicate in the cytoplasm, and exhibit early intercellular spread as a consequence of directional actin polymerization without detectable cellular injury (7–9).

Understanding the host response to *Rickettsia* infection has been advanced by the development of a standardized model of endothelial cell infection using primary human umbilical vein cells (HUVECs)[1] (10). In this model, infected endothelial cells have been shown to express cytokines, interferons, cell surface adhesion molecules such as E-selectin, VCAM-1, ICAM-1 (11–13), and $\alpha V\beta 3$ integrin (14), and pro-coagulants (tissue factor and von Willebrand factor) (15–17). These endothelial cellular responses explain aspects of the pathobiology of natural infections, including microvascular hemorrhage, endothelial leakage, and multiorgan failure (1).

An integrated understanding of the endothelial cellular response is not yet available. To address this question, we have undertaken a study of the global endothelial cell proteomic response to infection with *R. conorii* using quantitative proteomic profiling of *R. conorii*-infected HUVECs, including the analysis of plasma membrane and secreted proteins within the Golgi apparatus. Our experimental design was to use trypsin-mediated exchange of stable isotopes of H_2O to quantify differences in protein expression of primary HUVECs infected with *R. conorii versus* those stimulated with LPS alone to control for nonspecific inflammatory effects. In whole cellular lysates, we observed that *R. conorii*-infected endothelial cells significantly up-regulated the JAK-STAT signaling pathway. By contrast, analysis of PM and Golgi fractions revealed up-regulation of platelet adhesion proteins and down-regulation of integrin/cadherin components. To identify proteins secreted by *R. conorii*-infected HUVECs, soluble Golgi fractions were analyzed. Here, we observed significant induction of HLA and $\beta 2$-microglobulin, providing insights into major histocompatibility complex (MHC)-I-mediated antigen processing, important in the host cytotoxic T cell response. Finally, 34 rickettsial proteins were identified with high confidence in the Golgi apparatus, PM, or secreted protein fractions. These studies advance the understanding of the endothelial response to *R. conorii* infection through up-regulation of IFN- and MHC class I antigen presentation pathways and implications of the secretome for the host response and diagnostics.

[1] The abbreviations used are: HUVEC, human umbilical vein endothelial cell; FDR, false discovery rate; IPA, Ingenuity Pathway Analysis; PM, plasma membrane; SID, stable isotopic dilution; SRM, selected reaction monitoring; WCL, whole cell lysate; STAT, signal transducer and activator of transcription; NSAF, normalized spectral abundance factor; SAF, spectral abundance factor; ACN, acetonitrile; SIS, stable isotope standard.

EXPERIMENTAL PROCEDURES

Materials—Link sulfosuccinimidyl-2-(biotinamido) ethyl-1,3-dithiopropionate (Sulfo-NHS-SS-Biotin) was from Pierce (Thermo Scientific, San Jose, CA). NanoLink™ streptavidin magnetic beads (0.8 μm) were from Solulink, San Diego, CA (catalog no. M-1002); protease inhibitor mixture was from Sigma, St. Louis, MO (catalog no. P8340). LPS was from *Escherichia coli* 0111:B4 (Sigma).

Cell Cultures—Pools of HUVECs were established from individual human umbilical cords grown in supplemented EGM-2 medium (Lonza). The cells were subcultured when the monolayer became confluent two or three times per week. In this study, the cells were used between passages 3 and 4. For infection, 15×10^6 primary HUVECs in T175 flasks were infected in BSL-3 containment, and subsequently lysates were prepared 10 days later and were inactivated in accordance with University of Texas Medical Branch IBC-approved protocols. Cellular infection was verified by immunofluorescent microscopy using a rabbit polyclonal serum against *R. conorii* and anti-rabbit IgG conjugated to Alexa 594 (Life Technologies, inc.). HUVECs were stimulated with LPS (50 ng/ml) overnight as controls.

Rickettsia—R. conorii (Malish 7 strain) was obtained from the American Type Culture Collection (ATCC; Manassas, Va.; catalog no. VR-613). The stock, aliquots of a 10% suspension of infected yolk sac containing 4×10^6 pfu per ml, was stored at −70 °C.

Experimental Design and Statistical Rationale—HUVECs were infected with *R. conorii* and subjected to whole cell lysate, plasma membrane, and Golgi fractionation. Experiments were replicated twice. For each quantitative LC-MS/MS analysis, samples were subjected to label swapping as described below.

Plasma Membrane (PM) Preparation—LPS-stimulated or *R. conorii*-infected HUVECs were washed three times with PBS (37 °C) containing calcium and magnesium. PM proteins were cross-linked 15 min in 10 ml of PBS with 10 μl of EZ-Link Sulfo-NHS-SS-Biotin stock solution (100 mg/ml, freshly prepared in DMSO) as described previously (18). Afterward, cross-linker was quenched by addition of 5 ml of lysine solution (1 mg/ml), washed in ice-cold wash buffer (250 mM sucrose, 10 mM Tris, pH 7.4), and resuspended in ice-cold homogenization buffer (250 mM sucrose, 10 mM Tris, pH 7.4, 1:100 dilution of protease inhibitor (Sigma P8340), 1 mM NaF, and 1 mM Na_3VO_4). The cells were concentrated by centrifugation (10 min at $800 \times g$ at 4 °C), resuspended in homogenization buffer, and Dounce homogenized using 15 strokes of pestle A and 10 strokes of pestle B. The homogenate was then centrifuged (10 min at $1{,}000 \times g$, 4 °C), and membranes were captured by addition of suspended streptavidin magnetic beads (15 ml/T165 flask) followed by gentle mixing at 4 °C for 1 h and magnetic capture. The membrane-bound streptavidin beads were then washed with 1 M KCl (high salt wash) three times, followed by washing in 0.1 M Na_2CO_3, pH 11.5 (high-pH wash), and then ice-cold hypotonic buffer (10 mM HEPES, pH 7.5, 1.5 mM $MgCl_2$, 10 mM KCl, 1:100 dilution of protease inhibitor mixture, 1 mM NaF, and 1 mM Na_3VO_4). The streptavidin beads were resuspended in twice their volume of 2× SDS sample buffer containing 100 mM dithiothreitol

(DTT). After vortexing, beads were removed with a strong magnet, and the supernatant was saved. The proteins in the supernatant were separated by SDS-PAGE and visualized with Colloidal Blue (Life Technologies, Inc.). The gel in each lane was cut into small slices. The proteins were digested with trypsin in-gel as described previously. Briefly, the gel particles were destained in 1 ml of water/methanol solution (50:50, v/v) containing 25 mM NH_4HCO_3, pH 8.0, three times, changing the solution every 10 min. The destained gel was then washed in 1 ml of an acetic/methanol solution (acetic acid/methanol/water, 10:40:50, v/v/v) for 3 h, with the solution changed every 1 h. The resulting gel was soaked in 1 ml of water for 40 min, changing the solvent twice every 20 min. The gel was then transferred into a 0.5-ml microcentrifuge tube and dehydrated by soaking the gel in 100% acetonitrile (ACN) until it became opaque white. The solution was removed, and the gel was dried in a SpeedVac for 20–30 min. The dried gel was rehydrated with an adequate amount of trypsin digestion solution (10 ng of trypsin/μl in 50 mM NH_4HCO_3, pH 8.0). The digestion was carried out at 37 °C overnight. To extract tryptic digest, the gel was soaked in 40 μl of extraction solution (ACN/trifluoroacetic acid/water, 50:5:45, v/v/v) for 60 min with vortexing. The extraction solution was then carefully removed with a gel-loading pipette tip, and the extraction was repeated once. The extracts were pooled and dried with a SpeedVac. The tryptic peptides were used for trypsin-catalyzed ^{18}O labeling.

Golgi Preparation—Golgi preparations were performed as described (19). In brief, the flow-through of the magnetic bead separation from above was adjusted to a final concentration of 1.4 M sucrose by addition of 2.0 M sucrose and transferred to SW41 centrifuge tubes. Samples were overlaid with 4 ml of 1.2 M sucrose solution, topped off with 0.8 M sucrose solution, and spun at 38,000 rpm in an SW41Ti rotor (246,000 × g) for 90 min at 4 °C. Crude Golgi preparations were harvested from the 0.8/1.2 M sucrose interface. An aliquot was assayed for total protein concentration by the bicinchoninic acid (BCA) assay (Thermo Scientific).

Golgi Extracts—An equal volume of 1 M KCl was added to the crude Golgi preparation, incubated for 25 min with rotation at 4 °C, and an equal amount of ice-cold Dulbecco's modified PBS (D-PBS) added to each tube. The Golgi preparations were spun at 40,000 rpm (271,000 × *g*) at 4 °C. The membranes were then resuspended in 0.5 μl/μg of protein of crude extract using a 100 mM ammonium carbonate solution, pH 11.0. Membranes were removed by centrifugation at 40,000 rpm (271,000 × *g*) for 60 min at 4 °C. The soluble supernatants, representing the secreted proteins, were denatured by addition of an equal volume of 8 M guanidine HCl. Insoluble membranes were subjected to SDS-PAGE, and digested with trypsin in-gel as described above.

Trypsin Digestion of Whole Cell Lysate and Secreted Proteins—50 μg of protein were reduced with 10 mM DTT for 30 min at room temperature. Protein cysteinyl residues were alkylated with 30 mM iodoacetamide for 2 h at 37 °C. Each sample was diluted 1:10 with 100 mM ammonium bicarbonate and digested with 40 μg of trypsin overnight at 37 °C, and each tryptic peptide mixture was desalted with a Sep-Pak® C18 cartridge (Waters, Milford, MA) following the manufacturer's instructions. Peptides were eluted from the cartridge with 80% acetonitrile and completely dried using a Speedvac.

Trypsin-catalyzed $^{16}/^{18}O$ Labeling—The tryptic digest of each sample was divided into two parts of equal volume. One part was labeled with $[^{18}O]H_2O$, the other part remained unlabeled (^{16}O-H_2O). Peptide C-terminal $^{16}O/^{18}O$ labeling was performed as described previously (20, 21). The dried peptide samples were redissolved with 3 μl of anhydrous acetonitrile, 10 mg of immobilized trypsin (Applied Biosystems, CA), and 200 μl of normal water ($H_2{}^{16}O$) or heavy water $H_2{}^{18}O$ containing 50 mM ammonium bicarbonate was added to the *Rickettsia*-infected and LPS control peptides, respectively, and both samples were incubated for 48 h at 37 °C. Supernatants were collected using a spin column and mixed as follows: ^{18}O-labeled peptides from *Rickettsia*-treated sample mixed with ^{16}O-labeled peptides from LPS particle-treated sample (forward labeling); ^{16}O-labeled peptides from *Rickettsia*-treated sample mixed with ^{18}O-labeled peptides from LPS particle-treated sample (reverse labeling). After mixing, the samples were desalted with a SepPak C18 cartridge (Waters). The desalted peptides were stored at −80 °C for LC-MS/MS analysis.

LC-MS/MS Analysis—Dried peptide samples were redissolved in 2 μl of acetonitrile and diluted with 40 μl of 0.1% formic acid. LC-MS/MS analysis was performed with a Q Exactive Orbitrap mass spectrometer (Thermo Scientific, San Jose, CA) equipped with a nanospray source with an on-line Easy-nLC 1000 nano-HPLC system (Thermo Scientific, San Jose, CA). Ten microliters of each peptide solution were injected and separated on a reversed phase nano-HPLC C18 column (75 μm × 150 cm) with a linear gradient of 0–35% mobile phase B (0.1% formic acid, 90% acetonitrile) in mobile phase A (0.1% formic acid) over 120 min at 300 nl/min. The mass spectrometer was operated in the data-dependent acquisition mode with a resolution of 70,000 at full scan mode and 17,500 at MS/MS mode. The 10 most intense ions in each MS survey scan were automatically selected for MS/MS. The acquired MS/MS spectra were analyzed by 1.4 (22) using default parameters (supplemental File 1) in the Swiss-Prot human protein databases (downloaded on February 2013, 20,247 protein entries) using a mass tolerance of ±20 ppm for precursor and product ions and a static mass modification on cysteinyl residues that corresponded to alkylation with iodoacetamide. Differential modifications were defined to be ^{18}O-labeled C-terminal and oxidized methionine with a maximum of two missed cleavages. Protein identification data (accession numbers, peptides observed, sequence coverage) are in supplemental Tables 1–3. Annotated spectra of host proteins identified with single peptides are in supplemental file 2. Annotated spectra of rickettsial proteins identified with single peptides are in supplemental file 3. The FDR cutoff for peptide and protein identification is 0.01.

Data Processing—For each subcellular fraction, the experiments were repeated after swapping the ^{18}O-labeling between *Rickettsia*-infected cells and LPS-treated cells. This label swapping strategy allows for detection of irreproducible ratios that might arise due to interference in precursor quantification provided there is a minimum of two biological replicates. Each dataset was first centered by subtracting the most frequent value in that dataset and then subjected to MaxQuant Significant A analysis (22). Next, the forward and reverse datasets were plotted with forward log2 heavy/light (H/L) ratio (*x* axis) against reverse log2 H/L ratio (*y* axis). Only the proteins that have a Significant A *p* value below 0.05 and also located in either upper-left or lower-right quadrant are considered to be the significantly expressed proteins.

The normalized spectral abundance factor (NSAF) value for each protein was calculated as described (23) in Equation 1,

$$(NSAF)_k = \frac{\left(\frac{I}{L}\right)_k}{\sum_{i=1}^{N}\left(\frac{I}{L}\right)_i} \qquad \text{(Eq. 1)}$$

where the total MS intensity (*I*) of the matching peptides from protein *k* was divided by the protein length (*L*) and then divided by the sum of *I*/*L* for all uniquely identified proteins in the dataset.

Stable Isotope Dilution (SID)-selected Reaction Monitoring (SRM)-MS—The SID-SRM-MS assays were developed as described previously (24, 25). For each targeted protein, two or three peptides were initially selected and then the sensitivity and selectivity of these were experimentally evaluated as described previously (24, 25). The pep-

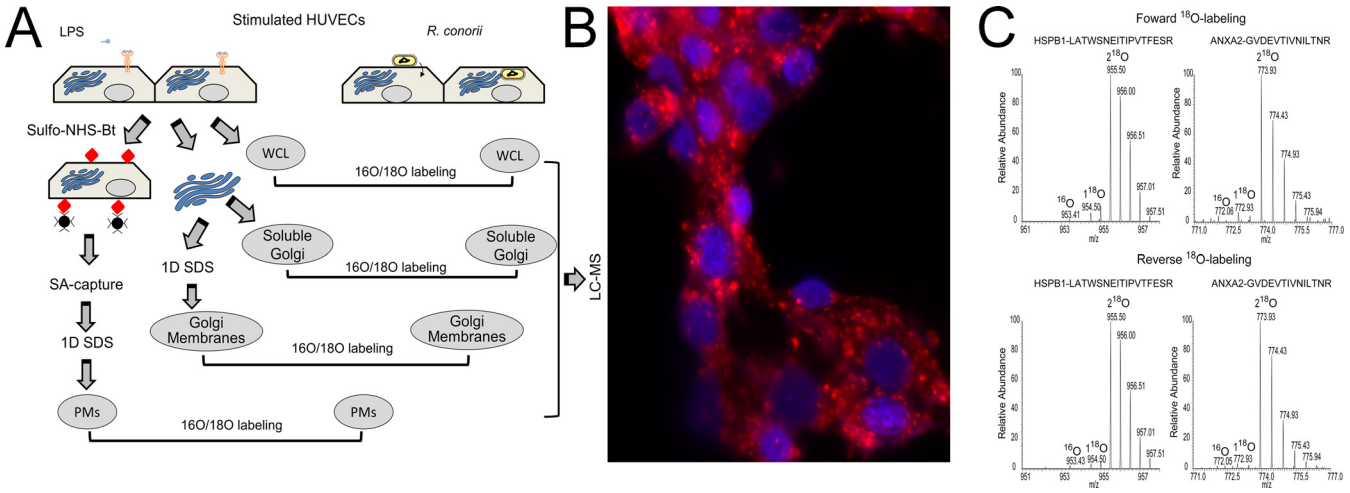

FIG. 1. **Quantitative proteomics study of *R. conorii* infection in HUVECs.** *A,* experimental strategy. Shown is a schematic diagram of the experimental work flow for the identification of differential protein expression control (LPS-stimulated) or *R. conorii*-infected HUVECs. *B,* immunofluorescence assay. Immunofluorescence assay for rickettsial antigen (*red*) and nuclear DNA (*blue*) in HUVECs smeared on a glass slide to determine rickettsial growth. Original objective magnification was ×40. The primary antibody was a rabbit anti-*R. conorii* immune serum. The secondary antibody was a donkey anti-rabbit labeled with Alexa 546. *C,* ^{18}O-labeling efficiency. MS spectra of two ^{18}O-labeled peptides (HSPB1, LATQSNEITIPVTFESR, and ANXA2, GVDEVTIVNILTNR) are shown.

tide with the best sensitivity and selectivity was selected as the surrogate for that protein. For each peptide, 3–5 SRM transitions were monitored. The signature peptides and SRM parameters are listed in Table VI. The peptides were chemically synthesized incorporating isotopically labeled [$^{13}C_6{}^{15}N_4$]arginine or [$^{13}C_6{}^{15}N_2$]lysine to a 99% isotopic enrichment (Thermo Scientific). The amount of stable isotope standard (SIS) peptides was determined by amino acid analysis. The tryptic digests were then reconstituted in 30 μl of 5% formic acid, 0.01% TFA. An aliquot of 10 μl of 50 fmol/μl diluted SIS peptides was added to each tryptic digest. These samples were desalted with a ZipTip C18 cartridge. The peptides were eluted with 80% ACN and dried. The peptides were reconstituted in 30 μl of 5% formic acid, 0.01% TFA and were directly analyzed by LC-SRM-MS. LC-SRM-MS analysis was performed with a TSQ Vantage triple quadrupole mass spectrometer equipped with nanospray source (Thermo Scientific, San Jose, CA). 8–10 targeted proteins were analyzed in a single LC-SRM run. The on-line chromatography was performed using an Eksigent NanoLC-2D HPLC system (AB SCIEX, Dublin, CA). An aliquot of 10 μl of each of the tryptic digests was injected on a C18 reverse-phase nano-HPLC column (PicoFrit™, 75 μm × 10 cm; tip inner diameter of 15 μm) at a flow rate of 500 nl/min over 20 min in 98% buffer A (0.1% formic acid), followed by a 15-min linear gradient from 2 to 30% mobile buffer B (0.1% formic acid, 90% acetonitrile). The TSQ Vantage was operated in high resolution SRM mode with Q1 and Q3 set to 0.2 and 0.7-Da full width half-maximum. All acquisition methods used the following parameters: 2100 V ion spray voltage, a 275 °C ion-transferring tube temperature, and a collision-activated dissociation pressure at 1.5 millitorr. The S-lens voltage used corresponded to the value in S-lens table generated during MS calibration.

All SRM data were manually inspected to ensure peak detection and accurate integration. The chromatographic retention time and the relative product ion intensities of the analyte peptides were compared with those of the SIS peptides. The variation of the retention time between the analyte peptides and their SIS counterparts should be within 0.05 min, and the difference in the relative product ion intensities of the analyte peptides and SIS peptides were below 20%. The peak areas in the extract ion chromatography of the native and SIS version of each signature peptide were integrated using Xcalibur® 2.1. The default values for noise percentage and baseline subtraction window were used. The ratio between the peak area of native and SIS version of each peptide was calculated.

Bioinformatics Analysis—High confidence protein identifications were subjected to pathway enrichment analysis using the Protein ANalysis THrough Evolutionary Relationship (Panther) pathway classification system (26). Pathways are rank-ordered based on statistically significant enrichment of the number of proteins in the dataset relative to the total number of proteins in the pathway. Ingenuity Pathway Analysis (IPA) was performed to identify relevant networks, rank-ordered by the number of proteins in the dataset relative to the pathway.

RESULTS

Experimental Design—To obtain a global understanding of the endothelial proteomics response to *Rickettsia* infections, we applied a standardized model developed by us using *R. conorii*-infected HUVECs, cells selected because they represent the primary target of *R. conorii* infection *in vivo*. Whole cell lysates (WCLs), PM, and Golgi fractions were prepared from uniformly *R. conorii*-infected primary HUVECs (Fig. 1*A*). In this experiment, conditions were established such that the cells were uniformly infected at the time of harvest (Fig. 1*B*). Quantitative stable isotopic labeling LC-MS/MS analysis was performed using trypsin-mediated ^{18}O exchange and was compared with LPS-stimulated HUVECs to control for inflammatory responses that are not specific to rickettsial infection.

For each pairwise comparison, the experiment was repeated after swapping the ^{18}O labeling between *R. conorii*-infected and LPS-stimulated HUVECs. Before the heavy- and light-labeled peptides were mixed, a small fraction of the ^{18}O-labeled sample was tested for ^{18}O-labeling efficiency with LC-MS/MS. Based on the analysis, the ^{18}O-labeling efficiency is higher than 95% based on the abundance of two ^{18}O-labeled peptides and their ^{16}O-labeled counterparts. For

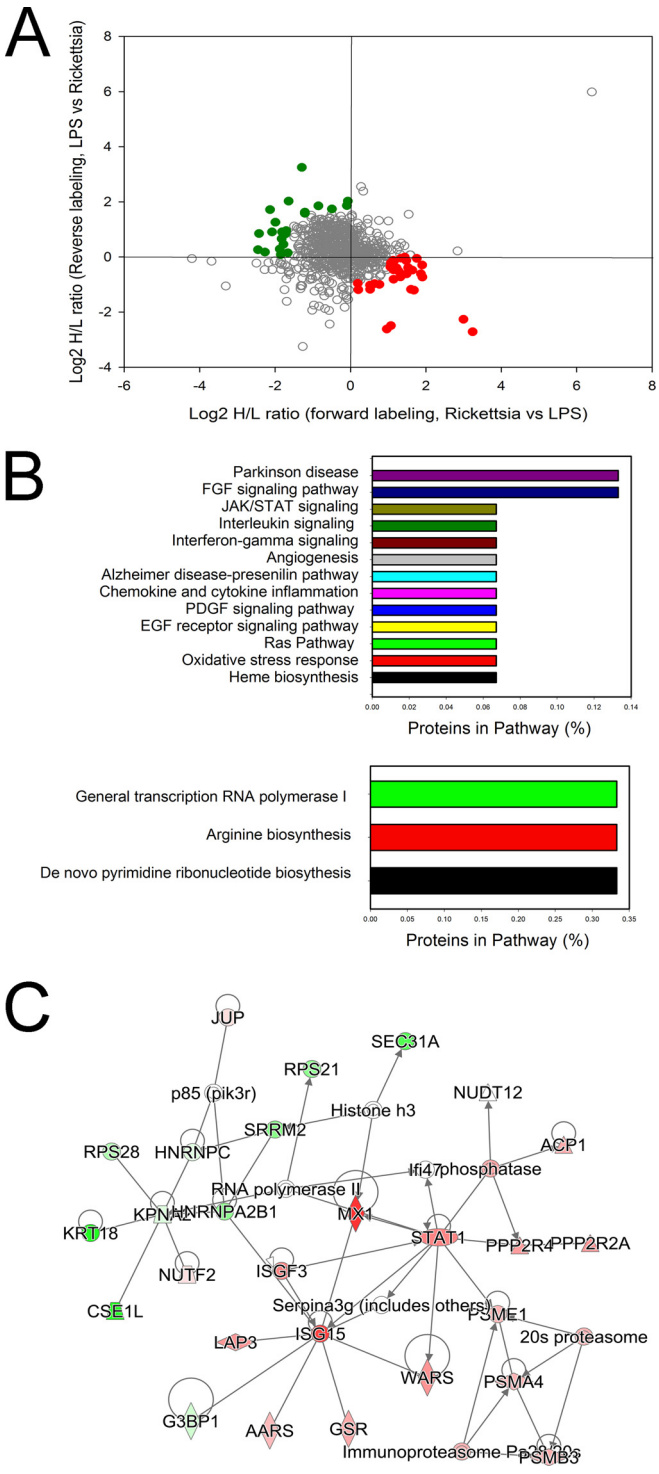

FIG. 2. **Differential protein expression in *R. conorii*-infected HUVEC WCLs.** *A*, quantification of regulation. The plots are $\log_2$-transformed forward and reverse heavy/light ratios of individual proteins quantitated in WCLs from each replicate. Up-regulated proteins identified from the *R. conorii*-infected HUVECs are located in the *bottom-right quadrant* (*red circles*), and the proteins down-regulated in *Rickettsia*-infected HUVECs are located in the *upper-left quadrant* (*green squares*). *B*, Panther pathway analysis. *Top panel,* top pathways for proteins enriched in HUVEC WCL identified by the Panther classification system. *x* axis is the percentage of the pathway represented in the identified proteins. *Bottom panel* is pathway analysis for proteins depleted in HUVEC WCLs. *C*, network by IPA. Shown is the top-ranked network of differentially expressed WCL proteins identified in the Ingenuity Knowledge base. For each node, *red* indicates up-regulation in *Rickettsia*-infected cells; *green*, down-regulation. For abbreviations, see Table I.

example, in the whole cell lysate ^{18}O quantification experiment, a total of 3,242 peptides were identified with 1% FDR by forward labeling. Among these, 3,127 (96.5%) were peptides with double-incorporated ^{18}O labels. Out of 5,938 peptides in the reverse labeling experiment, 5,845 (98.4%) were double-incorporated with ^{18}O labels. We further inspected the spectra manually. As shown in Fig. 1*C*, the ^{18}O-labeling efficiency was higher than 95% based on the abundance of two ^{18}O-labeled peptides and their ^{16}O-labeled counterparts.

Differentially Expressed Proteins Identified from WCLs—In WCLs, a total of 1,082 proteins were quantified in both the forward and reversed ^{18}O-labeling experiments, resulting in 784 high confidence proteins quantified (Fig. 2). A total of 55 proteins was differentially expressed (Fig. 2*A*), with 31 being up-regulated (Table I). The Pearson correlation of the quantitation of these significantly differentially expressed proteins between the two replicates is 0.68.

To understand the biological pathways affected by *R. conorii* infection, we subjected the data to pathway enrichment analysis using the Panther pathway classification system (see under "Experimental Procedures"). This classification is a simplified functional ontology of functional protein groups based on curated data linked by Hidden Markov Models, allowing for more accurate functional inferences (26). In this representation, pathways enriched in the data set are presented as a rank-ordered list based on the percentage of the proteins within the pathway that are represented in the observed data set. We noted that the 31 up-regulated proteins are found within 13 pathways (Fig. 2*B, top panel*); Parkinson disease, FGF signaling, JAK-STAT pathways, interleukin signaling, and chemokine/cytokine inflammation pathways are enriched. The pathways represented by the down-regulated proteins were RNA polymerase I, arginine biosynthesis, and *de novo* pyrimidine biosynthesis (Fig. 2*B, bottom panel*), suggesting that *R. conorii* infection significantly perturbs metabolic pathways in HUVECs.

IPA was performed on the 55 differentially expressed protein WCLs. One of the top-ranked networks enriched in this fraction was Molecular Transport and Protein Trafficking, containing a cluster of IFN-signaling proteins, including MX1, ISG3, STAT1, and ISG15 (Fig. 2C), consistent with the Panther pathway analysis.

Differentially Expressed PM Proteins—Previous work has shown that *R. conorii* induces significant changes in the expression of cell surface proteins, including tissue factor (16) and adhesion molecules (11–14), promoting a pro-thrombotic phenotype. Because PM proteins are under-represented in

TABLE I

Proteins with altered abundances in HUVEC WLCs

For each significantly regulated protein is shown the accession number (Acc #), protein name, common gene name, and mean heavy (H)/light (L) enrichment ratio for the stable isotopic quantification in the replicate measurements. The L/H ratio measured after the label swap experiment is also shown.

Acc #	Protein Name	Gene Name	Log 2 H/L ratio	
			Rickettsia (H) vs. LPS (L)	LPS (L) vs Rickettsia (H)
P20591	Interferon-induced GTP-binding protein Mx1	*MX1*	3.24	-2.71
P05161	Ubiquitin-like protein ISG15	*ISG15*	3.00	-2.26
P42224	Signal transducer and activator of transcription 1-alpha/beta	*STAT1*	1.91	-0.73
P53801	Pituitary tumor-transforming gene 1 protein-interacting protein	*PTTG1IP*	1.90	-0.30
P07602	Proactivator polypeptide	*PSAP*	1.87	-0.61
Q8TD55	Pleckstrin homology domain-containing family O member 2	*PLEKHO2*	1.76	-0.06
P23381	Tryptophan--tRNA ligase, cytoplasmic	*WARS*	1.68	-1.21
P63151	Serine/threonine-protein phosphatase 2A 55 kDa regulatory subunit B alpha isoform	*PPP2R2A*	1.64	-0.48
P28838	Cytosol aminopeptidase	*LAP3*	1.61	-1.18
Q15257	Serine/threonine-protein phosphatase 2A activator	*PPP2R4*	1.53	-0.39
P04080	Cystatin-B	*CSTB*	1.49	-0.61
Q15631	Translin	*TSN*	1.48	-0.13
P07339	Cathepsin D	*CTSD*	1.44	-0.01
P00390	Glutathione reductase, mitochondrial	*GSR*	1.34	-0.04
P24666	Low molecular weight phosphotyrosine protein phosphatase	*ACP1*	1.33	-0.72
Q14108	Lysosome membrane protein 2	*SCARB2*	1.28	-0.52
P49720	Proteasome subunit beta type-3	*PSMB3*	1.22	-0.40
P25789	Proteasome subunit alpha type-4	*PSMA4*	1.16	-0.14
Q06323	Proteasome activator complex subunit 1	*PSME1*	1.15	-0.81
P10768	S-formylglutathione hydrolase	*ESD*	1.14	-0.47
Q9NWV4	UPF0587 protein C1orf123	*C1orf123*	1.13	-0.12
P49588	Alanine--tRNA ligase, cytoplasmic	*AARS*	1.08	-0.22
O00244	Copper transport protein ATOX1	*ATOX1*	1.07	-2.49
P78417	Glutathione S-transferase omega-1	*GSTO1*	1.06	-0.36
Q7Z7A1	Centriolin	*CNTRL*	0.96	-2.62
Q92734	Protein TFG	*TFG*	0.77	-1.00
O76094	Signal recognition particle subunit SRP72	*SRP72*	0.64	-0.97
P14923	Junction plakoglobin	*JUP*	0.52	-1.18
P11766	Alcohol dehydrogenase class-3	*ADH5*	0.52	-1.02
P61970	Nuclear transport factor 2	*NUTF2*	0.21	-1.19
Q9BRF8	Calcineurin-like phosphoesterase domain-containing protein 1	*CPPED1*	0.19	-0.96
P52292	Importin subunit alpha-2	*KPNA2*	-0.07	2.03
P07910	Heterogeneous nuclear ribonucleoproteins C1/C2	*HNRNPC*	-0.10	1.86
Q13283	Ras GTPase-activating protein-binding protein 1	*G3BP1*	-0.49	1.74
P62857	40S ribosomal protein S28	*RPS28*	-0.85	1.85
P63220	40S ribosomal protein S21	*RPS21*	-1.21	1.62
P22626	Heterogeneous nuclear ribonucleoproteins A2/B1	*HNRNPA2B1*	-1.21	1.58
Q9UQ35	Serine/arginine repetitive matrix protein 2	*SRRM2*	-1.29	3.25
Q00341	Vigilin	*HDLBP*	-1.64	2.03
P62888	60S ribosomal protein L30	*RPL30*	-1.66	0.15
P27708	CAD protein	*CAD*	-1.71	0.95
Q6NZI2	Polymerase I and transcript release factor	*PTRF*	-1.72	0.84
Q9UBQ5	Eukaryotic translation initiation factor 3 subunit K	*EIF3K*	-1.78	0.45
P61353	60S ribosomal protein L27	*RPL27*	-1.82	0.91
P61604	10 kDa heat shock protein, mitochondrial	*HSPE1*	-1.83	0.66
Q13867	Bleomycin hydrolase	*BLMH*	-1.85	0.08
O94979	Protein transport protein Sec31A	*SEC31A*	-1.88	0.28
Q9Y3U8	60S ribosomal protein L36	*RPL36*	-1.99	1.26
P63173	60S ribosomal protein L38	*RPL38*	-2.08	0.90
Q9GZQ8	Microtubule-associated proteins 1A/1B light chain 3B	*MAP1LC3B*	-2.14	1.72
P10619	Lysosomal protective protein	*CTSA*	-2.27	0.18
P05783	Keratin, type I cytoskeletal 18	*KRT18*	-2.43	0.85
P55060	Exportin-2	*CSE1L*	-2.45	0.26

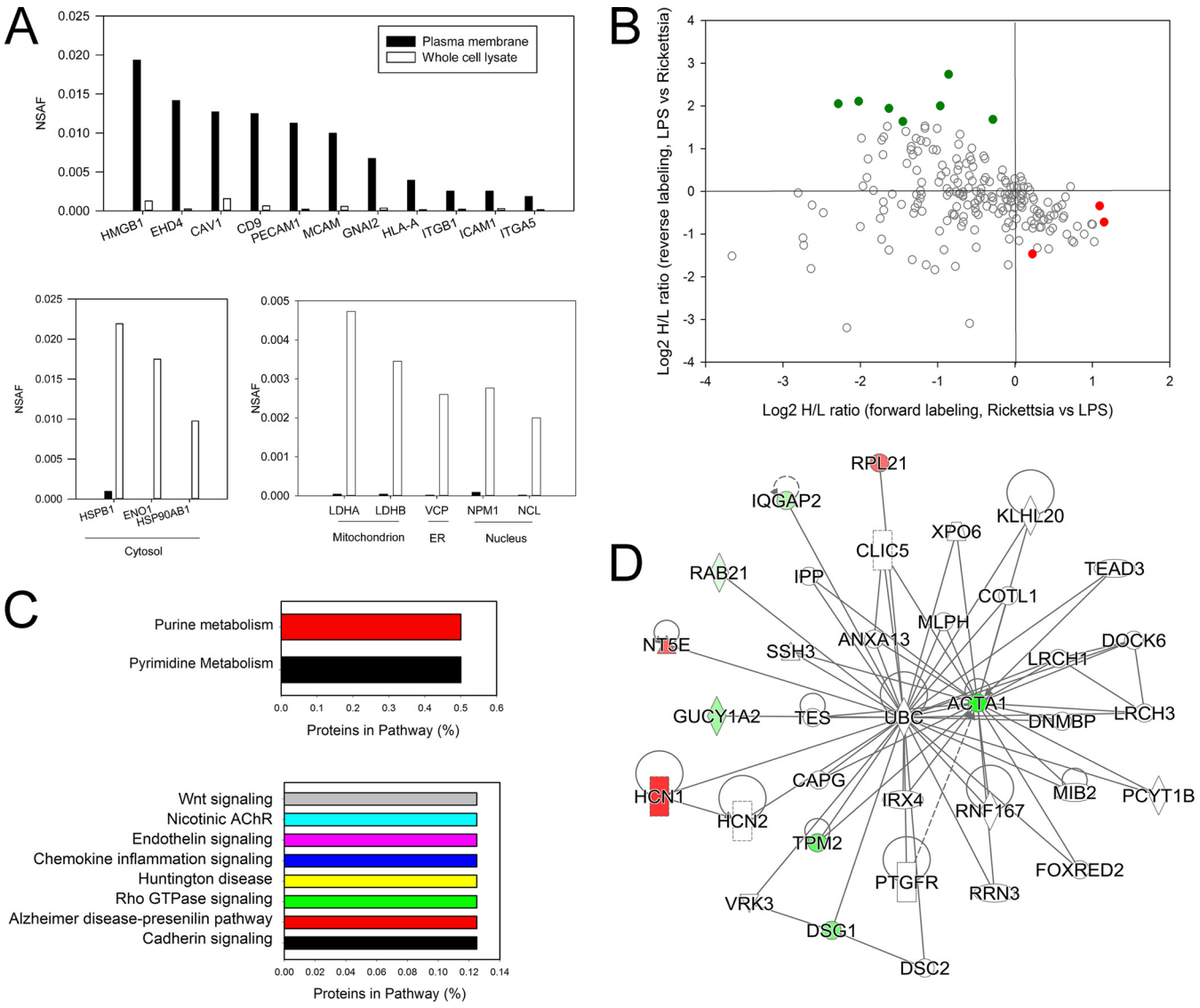

FIG. 3. **Differential protein expression in *R. conorii*-infected HUVEC PM fractions.** *A,* enrichment analysis. *Top,* spectral count measurements (NSAF) for representative plasma membrane proteins in the PM and WCL fractions. Note the enrichment of plasma membrane in the PM fractions. *Bottom left panel,* NSAF for cytosolic proteins, which are reduced (depleted) in PM fractions. *Bottom right panel,* NSAF for representative mitochondrial, endoplasmic reticulum, and nuclear proteins, also depleted in PM fractions. *B*, quantification of regulation. Shown are up-regulated proteins in PM fractions from *Rickettsia*-infected HUVECs in the *bottom-right quadrant* (*red*), and the proteins down-regulated in *Rickettsia*-infected HUVECs are located in the *top-left quadrant* (*green*). *C,* Panther pathway analysis. *Top panel*, highest ranked pathways identified by the Panther classification system for proteins enriched in HUVEC PMs. *Bottom panel*, pathways associated with down-regulated PM proteins. *D,* IPA network. Shown is the top-ranked network ("organismal disease") of PM proteins in the IPA Knowledge Base. Abbreviations are shown in Table II.

total cellular lysates, we separately analyzed the integral membrane proteome of R. *conorii*-infected HUVECs. For this purpose, we applied a biotin-directed affinity purification method developed by us for the preparation of integral PM proteins (18). A total of 286 plasma membrane proteins were quantified (Fig. 3). We used NSAF to confirm the enrichment of the plasma membrane proteins. NSAF is based on spectral counting, which has been widely used in label-free proteomics quantitation (27–29). In spectral counting, larger proteins usually generate more peptides and therefore more spectral counts than smaller proteins. Therefore, the number of spectral counts for each protein is first divided by the mass or protein length, which defines the spectral abundance factor (SAF). Furthermore, to accurately account for sample to sample variation, individual SAF values are normalized to one by dividing by the sum of all SAFs for proteins identified in the sample, resulting in the NSAF value (23). In this manner, NSAFs values are standardized across distinct samples, allowing direct comparisons to be made between individual samples. The NSAF value of one protein is positively corre-

TABLE II
Differentially expressed PM proteins

Acc #	Protein Name	Gene Name	Log 2 H/L ratio	
			Rickettsia (H) vs. LPS (L)	LPS (L) vs Rickettsia (H)
O60741	Potassium/sodium hyperpolarization-activated cyclic nucleotide-gated channel 1	*HCN1*	1.53	-0.19
P21589	5-nucleotidase	*NT5E*	1.15	-0.72
P46778	60S ribosomal protein L21	*RPL21*	1.09	-0.34
P62805	Histone H4	*HIST1H4A*	0.23	-1.47
Q9UL25	Ras-related protein Rab-21	*RAB21*	-0.29	1.68
Q13576	Ras GTPase-activating-like protein IQGAP2	*IQGAP2*	-0.86	2.74
P33402	Guanylate cyclase soluble subunit alpha-2	*GUCY1A2*	-0.97	2.00
Q02413	Desmoglein-1	*DSG1*	-1.45	1.63
P07951	Tropomyosin beta chain	*TPM2*	-1.63	1.94
P04745	Alpha-amylase 1	*AMY1A*	-2.02	2.11
P68133	Actin, alpha skeletal muscle	*ACTA1*	-2.29	2.05

lated with the relative abundance of the protein in this sample, where a highly abundant protein would have a higher NSAF value. We calculated the NSAF value for each protein identified in the PM fraction and whole cell lysate and then we compared their NSAF scores in the PM fraction and WCLs. As shown in Fig. 3*A*, compared with WCLs, plasma membrane proteins were highly enriched in the PM fraction, whereas the highly abundant cytosolic proteins HSP90AB1, HSPB1, and ENO1 were almost completely removed from our PM fraction. Proteins specific to the mitochondria (LDHA and LDHB), endoplasmic reticulum (VCP), and nucleus (NPM1 and NCL) were also significantly depleted from the PM fraction, indicating that we have successfully enriched the plasma membrane fraction.

Among 286 quantified PM proteins, a total of 11 differentially expressed proteins was identified (Fig. 3*B*). The Pearson correlation of the quantitation of these significantly differentially expressed proteins between the two replicates is 0.80. Four of these PM proteins were up-regulated by *R. conorii* infection (Table II). These proteins included hyperpolarization-activated potassium channel (HCN1) and 5′-nucleotidase. We noted that the most down-regulated PM protein was α-actin 1 (ACTA1), suggesting that *R. conorii* infection depletes PM ACTA1 as part of its effect on adherens junction formation and stress fiber formation *Rickettsia* (2, 8, 9, 30).

To more globally understand the functions controlled by this coordinated up-regulation of cell surface proteins, we subjected the differentially expressed proteins to enrichment analysis. Interestingly, proteins involved in purine and pyrimidine metabolism pathways were present in the up-regulated protein data set (Fig. 3*C, top panel*). Importantly, proteins controlling Wnt signaling, endothelin signaling, and cadherin signaling were in the down-regulated data set, among others (Fig. 3*C, bottom panel*). The effect of *R. conorii* on cadherin signaling may explain previously observed vascular leak phenomena and the effect on endothelial cell adherens junctions (1, 30). An IPA analysis showed a single network, "organismal disease" populated by down-regulated ACTA1 and the up-regulated HCN1 (Fig. 3*D*).

Differentially Expressed Golgi Proteins—Endothelial cells infected with *R. conorii* inducibly secrete a variety of soluble mediators. To better understand these, we profiled Golgi-enriched fractions containing proteins being processed for the secretory pathway. In this analysis, both total and soluble Golgi fractions were subjected to quantitative proteomic profiling. A total of 499 Golgi proteins were quantified; of these, 336 proteins were quantified in both experiments (supplemental Fig. 3). We used NSAF values to evaluate the enrichment of Golgi proteins and the proteins regulating the secretory pathways. As shown in Fig. 4*A*, Golgi apparatus protein 1 (GLG1) and several proteins of Golgi-derived retrograde transport vesicles such as SEC22B and three members of p24 family (TMED10, TMED3, and TMED7) were enriched in the Golgi fraction. Transmembrane emp24 domain-containing proteins are a widely conserved family of transmembrane proteins that play a functional role in protein transport within the early secretory pathway.

Among the 336 quantified proteins, a total of 52 differentially expressed proteins were identified (Fig. 4*B*), including 25 up-regulated proteins. The Pearson correlation of the quantitation of these significantly differentially expressed proteins between the two replicates is 0.88. These proteins included cell surface proteins PECAM, HLA-C, annexin, and others (Table III). We also noted interferon-induced transmembrane protein (IFITM)-3, consistent with the activation of the IFN-JAK-STAT signaling pathway observed in the WCL fractions. Enriched pathways of the up-regulated proteins in the Golgi membranes included GABA-type B protein receptor signaling and endogenous cannabinoid signaling (Fig. 4*C, top panel*).

The down-regulated proteins in the Golgi fractions represented Huntington disease, Rho GTPase, and cadherin-signaling pathways (Fig. 4*C, bottom panel*). The depletion of cadherins in the Golgi pathway is consistent with the reduction of cadherins in the PM fractions noted earlier. An IPA analysis showed a network linked to cell-cell signaling and cellular compromise, including von Willebrand factor, flotillin (FLOT1), annexin A2 (ANXA2), phospholipase D_3 (PLD3), HLA-C, and others (Fig. 4*D*).

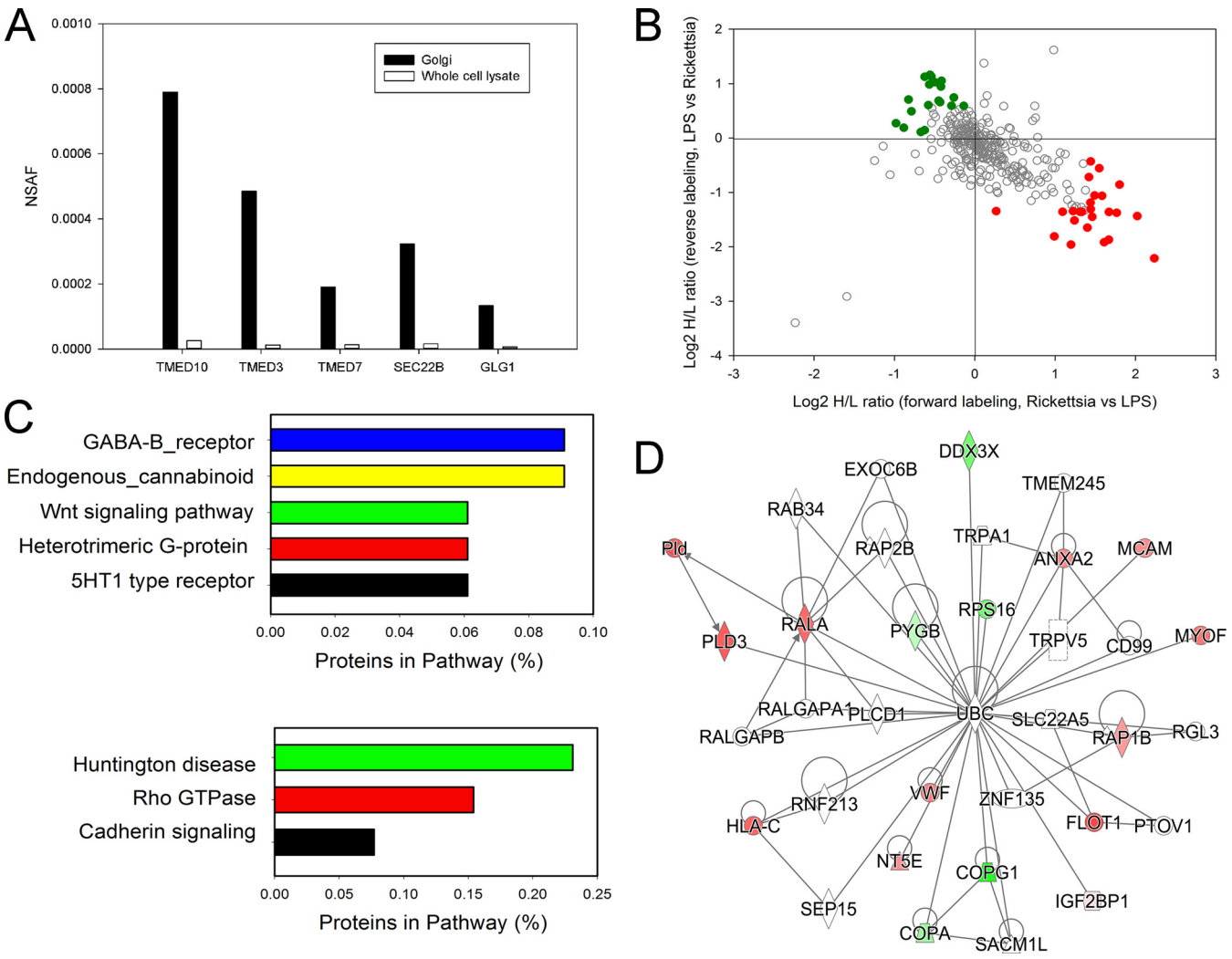

FIG. 4. **Differential protein expression in *R. conorii*-infected HUVEC Golgi fractions.** *A*, enrichment analysis. NSAF for selected Golgi proteins in HUVEC Golgi and WCL fractions. Note the high spectral counts in the Golgi fractions relative to that in WCL fractions. *B*, quantification of regulation. Golgi proteins up-regulated in *Rickettsia*-stimulated HUVECs are located in the *bottom-right quadrant* (*red*), the Golgi proteins down-regulated in *Rickettsia* stimulated cells are located in the *upper left* (*green*). *C,* Panther pathway analysis. *Top panel*, top ranked pathways for proteins enriched in HUVEC Golgi fractions. *Bottom panel,* pathway analysis for proteins depleted in HUVEC Golgi fractions. *D,* IPA network analysis. Shown is the top-ranked network ("cell-cell signaling and compromise") of Golgi proteins in IPA. Abbreviations are shown in Table III.

Differentially Expressed Soluble Golgi Proteins—To identify secreted proteins processed by the canonical secretory pathway, we separately analyzed changes in soluble Golgi protein proteomes; 371 proteins were identified in soluble Golgi extracts, with 216 proteins being quantified in both experiments (supplemental Fig. 4). We used NSAF values to evaluate the enrichment of secreted proteins in this fraction. As shown in Fig. 5*A*, extracellular proteins such as secreted protein, acidic, cysteine-rich (SPARC), fibronectin (FN1), Intercellular Adhesion Molecule (ICAM)-1, Connective Tissue Growth Factor (CTGF), Prosaposin (PSAP), and Golgi Glycoprotein 1 (GLG1) were enriched in this fraction. These proteins included HLA class I, PECAM, and β2-microglobulin (Table IV).

In the Golgi fraction, a total of 13 differentially expressed proteins were identified (Fig. 5*B*); of these, six were up-regulated by *Rickettsia* infection (Table V). The Pearson correlation of the quantitation of these significantly differentially expressed proteins between the two replicates is 0.86. To provide some biological insight into the activities of these secreted proteins, the up-regulated proteins were subjected to a protein class analysis. The most abundant protein activities of the secreted proteins were those encoding classes of cell adhesion/cell junction activity and hydrolase and protease activity (Fig. 5*C*). IPA analysis identified a pathway dominated by β2-microglobulin MHC class I and HLA isoforms (Fig. 5*D*).

Intracellular Distribution of Rickettsial Proteins—*Rickettsia* invade eukaryotic cells through an induced phagocytosis mechanism. The bacteria then escape from the phagosome and utilize actin filaments to spread (even to the nucleus) and

TABLE III
Golgi proteins with altered abundances in response to R. conorii infection and LPS stimulation

Acc #	Protein Name	Gene Name	Log 2 H/L ratio	
			Rickettsia (H) vs. LPS (L)	LPS (L) vs Rickettsia (H)
P16284	Platelet endothelial cell adhesion molecule	*PECAM1*	2.23	-2.21
O75955	Flotillin-1	*FLOT1*	2.02	-1.44
P17813	Endoglin	*ENG*	1.80	-0.86
Q8IV08	Phospholipase D3	*PLD3*	1.77	-1.37
P27105	Erythrocyte band 7 integral membrane protein	*STOM*	1.67	-1.36
P10321	HLA class I histocompatibility antigen, Cw-7 alpha chain	*HLA-C*	1.67	-1.87
P11233	Ras-related protein Ral-A	*RALA*	1.61	-1.92
Q01082	Spectrin beta chain, non-erythrocytic 1	*SPTBN1*	1.58	-1.06
P21796	Voltage-dependent anion-selective channel protein 1	*VDAC1*	1.55	-0.56
Q9NZM1	Myoferlin	*MYOF*	1.49	-1.05
P21926	CD9 antigen	*CD9*	1.46	-1.45
P08133	Annexin A6	*ANXA6*	1.44	-1.31
Q14108	Lysosome membrane protein 2	*SCARB2*	1.44	-0.43
P07339	Cathepsin D;Cathepsin D light chain;Cathepsin D heavy chain	*CTSD*	1.44	-1.19
Q01628	Interferon-induced transmembrane protein 3	*IFITM3*	1.42	-0.72
P04275	von Willebrand factor;von Willebrand antigen 2	*VWF*	1.40	-1.65
Q02818	Nucleobindin-1	*NUCB1*	1.33	-1.36
P07355	Annexin A2	*ANXA2*	1.31	-1.36
P43121	Cell surface glycoprotein MUC18	*MCAM*	1.24	-1.52
P04899	Guanine nucleotide-binding protein G(i) subunit alpha-2	*GNAI2*	1.22	-1.34
P21589	5-nucleotidase	*NT5E*	1.20	-1.96
P61224	Ras-related protein Rap-1b	*RAP1B*	1.09	-1.36
P62879	Guanine nucleotide-binding protein G(I)/G(S)/G(T) subunit beta-2	*GNB2*	0.99	-1.81
Q9NZI8	Insulin-like growth factor 2 mRNA-binding protein 1	*IGF2BP1*	0.27	-1.34
P14174	Macrophage migration inhibitory factor	*MIF*	-0.14	0.59
P60981	Destrin	*DSTN*	-0.26	0.74
P11216	Glycogen phosphorylase, brain form	*PYGB*	-0.29	0.59
P04632	Calpain small subunit 1	*CAPNS1*	-0.41	1.05
P05783	Keratin, type I cytoskeletal 18	*KRT18*	-0.42	0.94
P13639	Elongation factor 2	*EEF2*	-0.43	0.66
P53621	Coatomer subunit alpha;Xenin;Proxenin	*COPA*	-0.45	0.68
P81605	Dermcidin;Survival-promoting peptide;DCD-1	*DCD*	-0.50	1.02
P17066	Heat shock 70 kDa protein 6	*HSPA6*	-0.54	1.13
P68133	Actin, alpha skeletal muscle	*ACTA1*	-0.56	1.16
P07900	Heat shock protein HSP 90-alpha	*HSP90AA1*	-0.57	0.98
P49327	Fatty acid synthase	*FASN*	-0.58	0.60
Q13509	Tubulin beta-3 chain	*TUBB3*	-0.62	1.12
O00571	ATP-dependent RNA helicase DDX3X	*DDX3X*	-0.62	0.14
P62249	40S ribosomal protein S16	*RPS16*	-0.67	0.11
Q16851	UTP--glucose-1-phosphate uridylyltransferase	*UGP2*	-0.79	0.49
Q01995	Transgelin	*TAGLN*	-0.82	0.71
P09486	SPARC	*SPARC*	-0.88	0.19
Q9Y678	Coatomer subunit gamma-1	*COPG1*	-0.98	0.27

replicate in the host cell cytoplasm and nucleus. However, the subcellular distribution of *Rickettsia* proteins has not yet been determined to our knowledge. Unmatched spectra from our proteomics study were searched against the *Rickettsia* proteome database (downloaded from SwissProt protein database on February 20, 2013, 4,189 entries); 34 proteins were identified with a false discovery rate estimation of 1% or less in the PM, Golgi, and secreted protein fractions (Table V). These proteins show a characteristic non-random distribution. For example, the *Rickettsia* chaperone proteins, HtpG, DnaK, NADPH reductase, and cytosolic aminopeptidase, were enriched in the Golgi fractions, consistent with either contamination of Golgi fraction with *Rickettsia* organisms or biological processing of rickettsial proteins by the host Golgi pathway. The cytochrome *c* oxidase and NADH-quinone oxidoreductases were observed in the Golgi preparations, perhaps suggesting that these molecules may be a source of enhanced superoxide and lipid peroxidation observed in *Rickettsia*-infected endothelial cells (31).

A large number of *R. conorii* proteins was identified in the soluble fraction of the Golgi preparation and some of these included ferredoxin, heme biosynthetic enzymes, peptide chain releasing factors, protein translocases, and others (Table V). In the soluble Golgi fractions, we also identified the cell surface antigen Sca2, a formin mimic responsible for interacting with the host actin cytoskeleton (32). Finally, a distinct group of *R. conorii* proteins was identified in HUVEC plasma membrane fractions; these proteins were putative ligases, dehydrogenases, glycoprotein transferases, and lipoprotein-metabolizing proteins (Table V).

Verification of Host- and Rickettsial Proteins—To qualify the differential expression of endothelial innate response

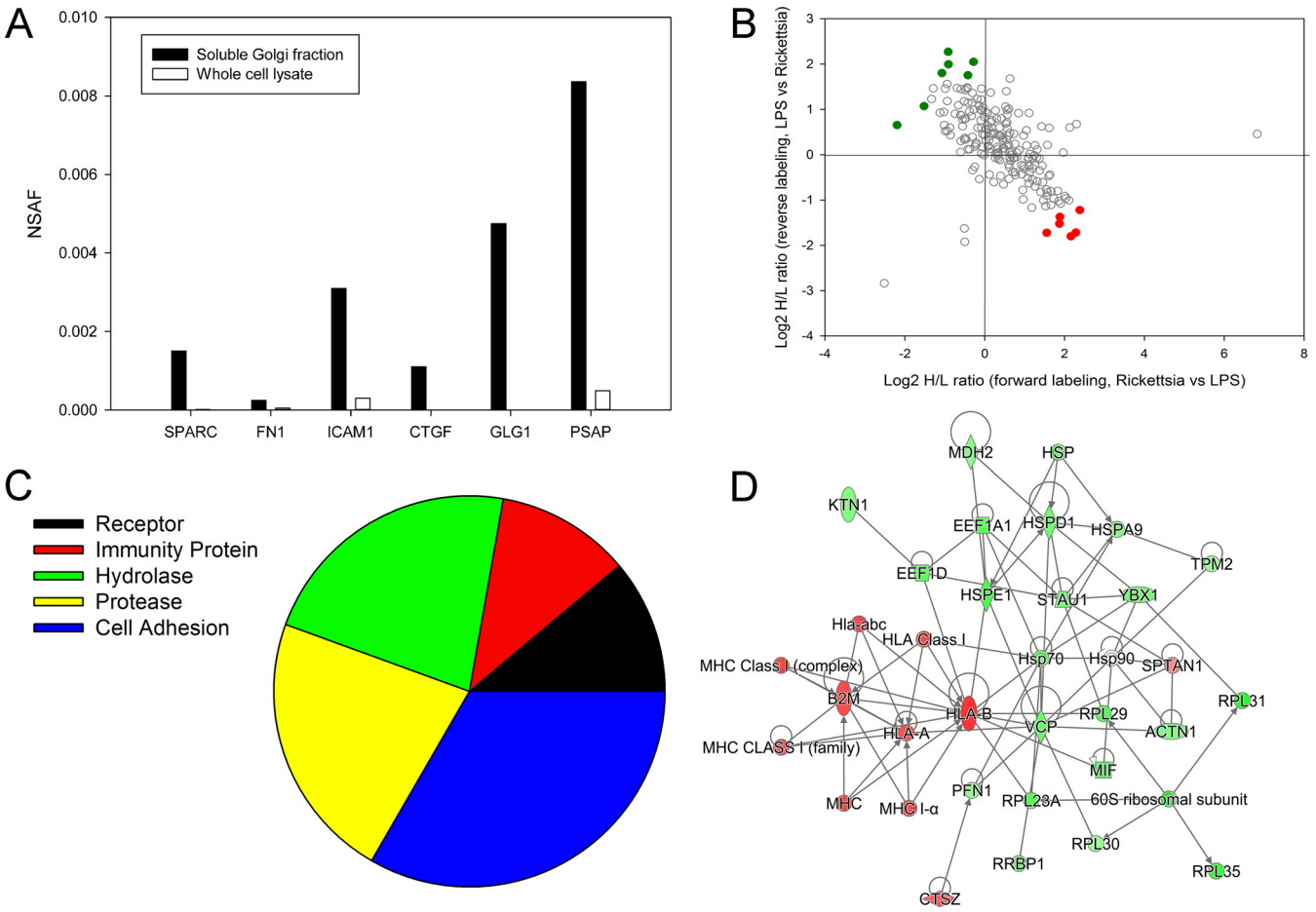

FIG. 5. **Differential expression of secreted proteins in *R. conorii* infection.** *A*, enrichment analysis. NSAF for selected secreted proteins in soluble Golgi fraction relative to WCL fractions. Note the high spectral counts in the soluble fractions relative to that in WCLs. *B*, quantification of regulation. Secreted proteins identified in soluble Golgi fraction. Proteins up-regulated in *Rickettsia*-infected HUVECs are located in the *bottom-right quadrant* (*red*), and down-regulated proteins are located in the *upper left* (*green*). *C*, Panther protein classification. Shown are the protein classifications for the secreted proteins in the *R. conorii*-infected HUVECs. *D,* IPA network. Shown is the top-ranked network ("immunological disease") of soluble Golgi proteins from IPA. Abbreviations are shown in Table IV.

TABLE IV
Soluble Golgi proteins

Acc #	Protein Name	Gene Name	Log 2 H/L ratio	
			Rickettsia (H) vs. LPS (L)	LPS (L) vs Rickettsia (H)
P01892	HLA class I histocompatibility antigen, A-2 alpha chain	*HLA-A*	2.38	-1.22
P30480	HLA class I histocompatibility antigen, B-42 alpha chain	*HLA-B*	2.28	-1.72
P51688	N-sulphoglucosamine sulphohydrolase	*SGSH*	2.16	-1.80
Q9UBR2	Cathepsin Z	*CTSZ*	1.88	-1.38
P16284	Platelet endothelial cell adhesion molecule	*PECAM1*	1.87	-1.53
P61769	Beta-2-microglobulin;Beta-2-microglobulin form pI 5.3	*B2M*	1.55	-1.73
P47914	60S ribosomal protein L29	*RPL29*	-0.28	2.05
P29692	Elongation factor 1-delta	*EEF1D*	-0.42	1.75
P62899	60S ribosomal protein L31	*RPL31*	-0.91	2.00
P02452	Collagen alpha-1(I) chain	*COL1A1*	-0.91	2.27
P42766	60S ribosomal protein L35	*RPL35*	-1.07	1.80
Q9NQC3	Reticulon-4	*RTN4*	-1.52	1.07
P18859	ATP synthase-coupling factor 6, mitochondrial	*ATP5J*	-2.20	0.65

TABLE V
R. conorii proteins identified
Each protein is identified with FDR of <1%. For each protein, the subcellular fraction in which it was identified is shown.

Accession	Protein Name	Gene Name	Golgi	Plasma membrane	Golgi soluble fraction
A8EB9	UvrABC system protein C	*uvrc*	+		+
A8EL6	Probable transcriptional regulator protein A1E_02520	*a1e_02520*			+
A8EZN6	Exodeoxribonuclease 7 large subunit	*xsea*		+	
A8GMB3	Aspartate tRNA ligase	*asps*		+	+
A8GMF9	Chaperone protein DnaK	*dnak*	+		
A8GMX2	DNA mismatch repair protein MutS	*muts*		+	
A8GQ51	Chaperone protein HtpG	*htpg*	+	+	
A8GVS7	Valine tRNA ligase	*vals*		+	
A8GXR2	Ubiquinone/menaquinone biosynthesis methltransferase ubiE	*ubie*	+	+	
B0BWT1	Heme A synthase	*ctaa*			
C4K2V3	Glycine tRNA ligase beta subunit	*glys*			
Q1RI31	Putative ankyrin repeat protein RBE_0902	*rbe_0902*			+
Q1RIZ4	Putative ankyrin repeat protein RBE_0589	*rbe_0589*		+	
Q1RK13	Putative ankyrin repeat protein RBE_0220	*rbe_0220*		+	
Q4UL18	Ribosomal RNA small subunit methyltransferase H	*rsmh*		+	
Q4UL32	Putative fatty acid oxidation complex trifunctional enzyme	*rf_0890*			+
Q4ULJ8	ADP,ATP carrier protein 4	*tlcd*		+	
Q4UNA0	DNA topoisomerase 4 subunit A	*parc*			+
Q4UNB1	Phosphate acetyltransferase	*pta*			+
Q68WL4	30S ribosomal protein S1	*rpsa*	+		
Q68WP2	P+ruvate, phosphate dikinase	*ppdk*			+
Q68X04	Lysine tRNA ligase	*lyss*		+	
Q68X64	Histidine tRNA ligase	*hiss*	+		
Q68XE8	Threonine tRNA ligase	*thrs*			+
Q68XE8	Threonine tRNA ligase	*thrs*		+	
Q68XQ6	DNA replication and repair protein RecF	*recf*		+	
Q6TUJ8	Protein translocase subunit SecA	*seca*			+
Q92G41	Ferredoxin	*fdxa*			+
Q92G99	NADH quinone oxidoreductase subunit J	*nuoj*		+	
Q92JF7	Putative surface cell antigen sca2	*sca2*			+
Q9ZD55	Pyruvate, phosphate dikinase	*ppdk*		+	
Q9ZDM1	tRNA specific 2 thiouridylase MnmA	*mnma*		+	
Q9ZDM3	Cytochrome c oxidase assembly protein CtaG	*ctag*	+		

TABLE VI

SID-SRM-MS assays for human and rickettsial proteins

For each protein, the proteotypic peptide (sequence) is shown, along with the mass to charge ratio (*m/z*) for the first quadrupole (Q1) and third quadrupole (Q3) measurement, the ion type, and optimized collision energy.

Protein Name	Uniprot Accession #	Gene Name	Sequence	Q1 (m/z)	Q3 (m/z)	Ion type	Collision Energy (V)
Rickettsial Proteins							
UvrABC system protein C (*Rickettsia*)	A8EYB9	*uvrc*	ELFDLSEIPER	674.343	401.214	y3	26
				674.343	843.457	y7	26
				674.343	730.372	y6	26
				674.343	958.484	y8	26
Putative ankyrin repeat protein RBE (*Rickettsia*)	Q1RI31	*y902*	DGDTALTWAASSGLEK	811.389	1049.526	y10	30
				811.389	948.478	y9	31
				811.389	1162.610	y11	29
Chaperone protein HtpG (*Rickettsia*)	A8GQ51	*htpg*	EDLIDNLGTIAR	665.354	859.463	y8	26
				665.354	744.436	y7	26
				665.354	972.547	y9	26
				665.354	1085.631	y10	25
Host (Human) Proteins							
HLA class I histocompatibility antigen	P01892	*1A02*	FIAVGYVDDTQFVR	815.417	979.484	y8	31
				815.417	880.415	y7	31
				815.417	1142.547	y9	30
				815.417	1199.569	y10	29
Ubiquitin-like protein ISG15	P05161	*ISG15*	LAVHPSGVALQDR	681.878	758.415	y7	26
				681.878	845.447	y8	26
				681.878	1079.559	y10	26
				681.878	942.500	y9	26
Signal transducer and activator of transcription 1-alpha/beta	P42224	*STAT1*	ELSAVTFPDIIR	680.877	613.366	y5	26
				680.877	760.435	y6	26
				680.877	861.482	y7	26
				680.877	960.551	y8	26

proteins, we developed quantitative high throughput SRM assays to selectively measure each protein. The proteins, gene names, and accession numbers are shown in Table VI. The optimal empirically determined collision energy is also tabulated. Compared with LPS-stimulated cells, significant induction of STAT1 and ISG15 was observed in the WCL (Fig. 6*A*).

We also selected candidate rickettsial proteins identified in the Golgi and PM fractions as follows: the putative UvrABC system protein C; putative ankyrin repeat protein RBE; and chaperone protein HtpG. Compared with LPS-stimulated cells, significant induction of each was observed (Fig. 6*B*). The up-regulation of HLA proteins and the rickettsial proteins UVRVC and HPTG in the soluble Golgi fraction was also confirmed with SID-SRM-MS (Fig. 6*C*).

DISCUSSION

Rickettsiae are non-motile, Gram-negative, and obligately intracellular bacterial pathogens of global medical and veterinary health importance. During transmission, an infected hematophagous arthropod vector introduces rickettsiae into the dermis, where the organism disseminates to vascular endothelial cells throughout the body. Here, dividing *Rickettsia* induce cellular stress leading to cell detachment. Detached endothelial cells, which are heavily infected, lodge into downstream capillaries and initiate new foci of vascular infection. In our approach, we harvested infected endothelial cells once they were homogeneously infected, which mimic these foci of vascular infection. Such multifocal lesions are found throughout the course of the disease, even at early stages. We applied subcellular fractionation and quantitative proteomics to develop an integrated understanding of the human endothelial cellular response and subcellular distribution of *Rickettsia* proteins in this model of established infection. We deduced the activation of the JAK-STAT-ISG15 signaling pathway along with significant perturbations of cell surface enzymatic activities of infected endothelial cells. We think it important that *R. conorii*-infected endothelial cells show significant down-regulation of cadherin components whose putative role in pathogenesis is discussed below.

Previous work by us has shown that the IFN response is a major determinant limiting severity of rickettsial disease *in vivo* (33, 34). Although the pattern recognition receptors for rickettsial infection are not fully understood, replication of *Rickettsia* is a stimulus for production of type I IFN (IFNβ) (35). The type I IFN response has been observed as a common response to *Rickettsia* infections for all endothelial cell types

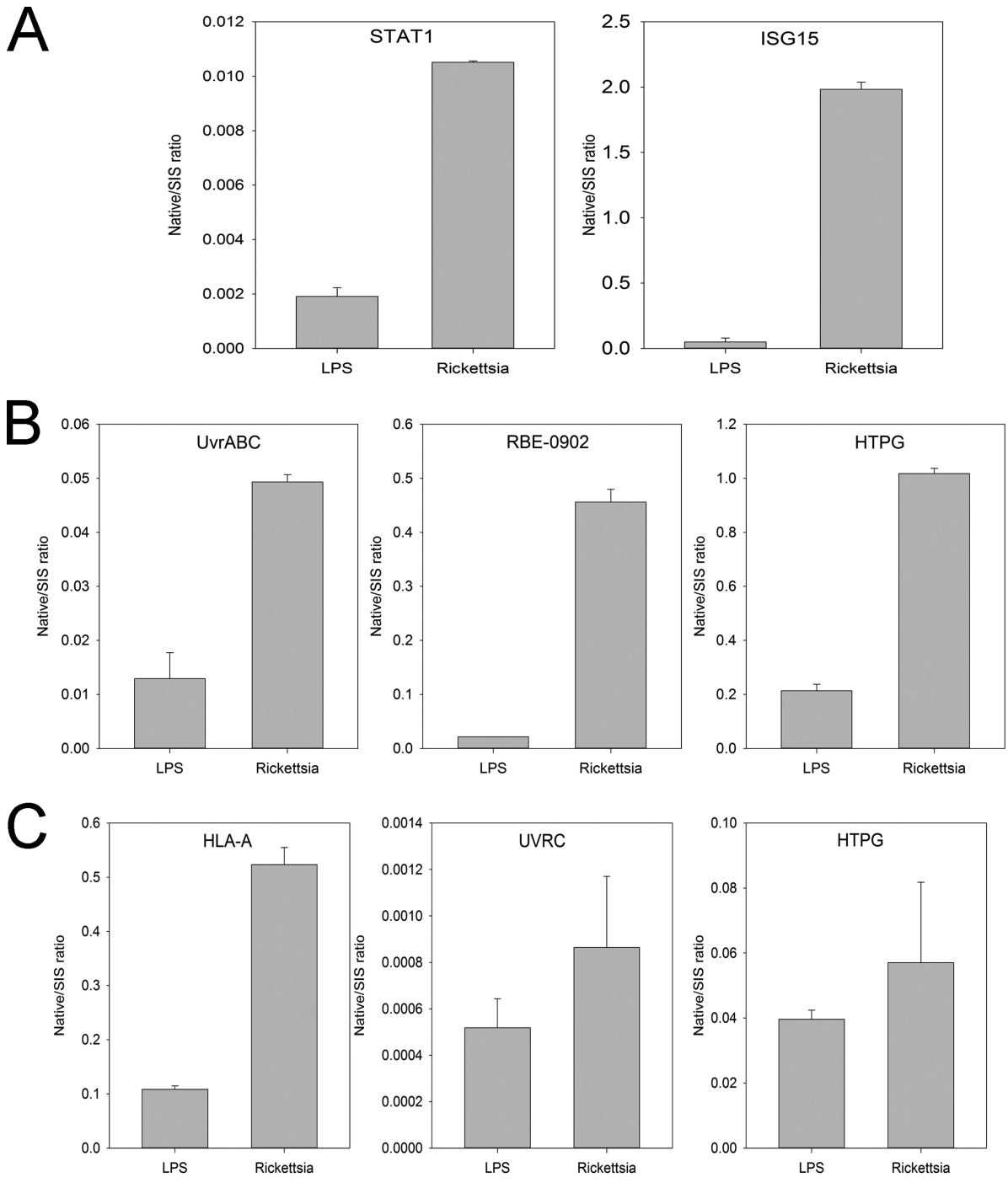

FIG. 6. **Qualification of innate response proteins in *R. conorii*-infected HUVECs.** *A*, qualification of IFN pathway. Shown are SID-selected reaction-monitoring (*SRM*)-MS measurements of STAT1 and ISG15 (*bottom*) for HUVEC stimulated with LPS (*left*) or infected with *R. conorii* (*right*). *y* axis is ratio of protein relative to internal SIS peptide (native/SIS) peptide (native/*aqua*). *B*, qualification of rickettsial proteins in Golgi membranes. SID-SRM-MS measurements for UvrABC system protein C are shown; putative ankyrin repeat protein RBE; and chaperone protein HtpG. Compared with LPS-stimulated cells, significant induction of each was observed. *C,* qualification of rickettsial proteins in soluble Golgi fraction. SID-SRM-MS measurements for human HLA proteins and the rickettsial proteins UVRVC and HPTG in the soluble Golgi fraction.

examined (36). Downstream of IFN, activation of the STAT1 signaling pathway triggers production of ISG, MX1, SOCS, and other proteins important in host defense (37). ISG15 is a small ubiquitin-like modifier induced at the transcriptional level by IFN signaling known to covalently modify target proteins by ISGylation, inducing changes in signaling, chemotaxis, and translation. In human microvascular endothelial cells infected with *R. conorii*, ISG15 is up-regulated through

an IFN-β-dependent pathway, and it controls intracellular rickettsial replication (35). Our data extend the *Rickettsia*-induced IFN pathway to include intracellular MX1 and cell-surface associated IFITM3 expression. More study will be required to understand their role, if any, in restricting rickettsial infection.

Previous work has shown that E-selectin (11), VCAM-1, ICAM-1 (11–13), and αVβ3 integrin (14) are plasma membrane proteins up-regulated in *Rickettsia*-infected cells to mediate neutrophil attachment, as well as vascular integrity. Because of their size, hydrophobic characteristics, and insolubility, the analysis of PM proteins is typically challenging. In this study, we applied a cell surface-directed biotin cross-linking method to affinity-enrich PM proteins in *Rickettsia*-infected cells. This method enables the enrichment and quantitation of integral PM proteins (18). Our data suggest that rickettsial infection up-regulates voltage channels in endothelial cell and depletes plasma membrane-associated ACTA1. Such changes could underlie vascular reactivity and the phenomenon of endothelial cell detachment (38), which could be a source of new foci of infection once they lodge in distal capillaries.

Previous studies provided evidence that T lymphocytes are critical in the development of immune protection in rickettsial disease; CD4 and CD8 T lymphocytes protect mice against lethal disseminated endothelial infection with *R. conorii* (39), but CD8 T cells are the most critical effectors (40). We note that up-regulation of HLA-I antigen transporter is observed, along with the presence of β2-microglobulin, hydrolases, and *Rickettsia* OmpB (Sca5) and Sca2 in the secretory pathway (soluble Golgi fraction). Importantly, OmpB is an immunodominant antigen for CD8 T lymphocytes in a mouse model of *R. conorii* infection (41). These data may explain how this immunodominant rickettsial antigen is processed and presented to the PM.

von Willebrand factor (vWF), an adhesive glycoprotein involved in primary hemostasis, is primarily stored in endothelial secretory granules, Weibel-Palade bodies, from which it is released during rickettsial infection (42). We observe increased abundance of vWF in *R. conorii*-infected endothelial cells. These data may suggest that newly synthesized vWF is processed by the Golgi apparatus prior to its packaging within the Weibel-Palade body.

Analysis of the soluble fraction of Golgi-enriched organelles provides a number of insights into the host response of endothelial cells. Endothelial host response proteins are highly enriched in MHC class I activity, including HLA-A, -C, and β2-microglobulin. Interestingly, *Rickettsia* cell surface antigens, Sca-5 and -2, are found in the secretory pathway, which may be a reflection of antigenic processing for presentation through the MHC class I pathway. Previous work by us has shown that MHC I knockout mice are highly susceptible to rickettsial infection due to defects in mobilizing an efficient cytotoxic T cell response (40). Interestingly, we have observed that cathepsin is an abundant cysteine protease enriched in the secretory fraction. Cathepsin has recently been shown to be involved in proteolytic processing of chemerin to trigger migration of human blood-derived plasmacytoid dendritic cells (43). Whether cathepsin plays a role in host response to *Rickettsia* infection may be an important direction for future research.

Our experimental design was intended to identify the major responses of human endothelial cells to established rickettsial infection. In our design, we harvested infected endothelial cells once they were homogeneously infected, a model that mimics foci of vascular infection from detached endothelial cells important in rickettsial dissemination. Other mechanistic studies have shown rapid activation of STAT3 signaling within hours of rickettsial infection, followed by a later activation of STAT1 (44). More work will be required to understand the early patterns of host response in rickettsial infection.

In summary, our study provides an integrated host and bacterial proteomics analysis of the infection of primary human endothelial cells with the etiologic agent of human Mediterranean spotted fever, *R. conorii*. Our study identifies the STAT1-ISG15 and HLA antigen production as the major components of the innate and adaptive immune response triggered by endothelial cells. We observe significant reprogramming of the plasma membrane proteome and induction of adhesion molecules, with down-regulation of endothelial cell cadherins. These observations generate insights into how rickettsiae induce the endothelial stress response.

* This work was supported by NIAID Clinical Proteomics Center Grant HHSN272200800048C (to A.R.B.), University of Texas Medical Branch Clinical and Translational Science Award (CTSA) UL1TR000071 (to A.R.B.), and NIEHS Grant P30 ES006676 (to A.R.B.). The authors declare that they have no conflicts of interest with the contents of this article. The content is solely the responsibility of the authors and does not necessarily represent the official views of the National Institutes of Health.

This article contains supplemental Files 1–3, Tables 1–3, and Figs. 1–4.

¶¶ To whom correspondence should be addressed: Tel.: 409-772-1950; Fax: 409-772-8709, E-mail: arbrasie@utmb.edu.

Data deposition Repository: ProteomeXchange Consortium; **Project Name:** Endothelial cell proteomic response to Rickettsia conorii infection; **Project accession:** PXD002650 **Reviewer account details: Username:** reviewer72296@ebi.ac.uk **Password:** PSZLXnUC.

REFERENCES

1. Walker, D. H., Valbuena, G. A., and Olano, J. P. (2003) Pathogenic mechanisms of diseases caused by *Rickettsia*. *Ann. N.Y. Acad. Sci.* **990,** 1–11
2. Walker, T. S., and Winkler, H. H. (1978) Penetration of cultured mouse fibroblasts (L cells) by *Rickettsia prowazeki*. *Infect. Immun.* **22,** 200–208
3. Martinez, J. J., and Cossart, P. (2004) Early signaling events involved in the entry of *Rickettsia conorii* into mammalian cells. *J. Cell Sci.* **117,** 5097–5106
4. Chan, Y. G., Cardwell, M. M., Hermanas, T. M., Uchiyama, T., and Martinez, J. J. (2009) Rickettsial outer-membrane protein B (rOmpB) mediates bacterial invasion through Ku70 in an actin, c-Cbl, clathrin, and caveolin 2-dependent manner. *Cell. Microbiol.* **11,** 629–644
5. Renesto, P., Dehoux, P., Gouin, E., Touqui, L., Cossart, P., and Raoult, D. (2003) Identification and characterization of a phospholipase D-superfamily gene in rickettsiae. *J. Infect. Dis.* **188,** 1276–1283

6. Whitworth, T., Popov, V. L., Yu, X. J., Walker, D. H., and Bouyer, D. H. (2005) Expression of the *Rickettsia prowazekii* pld or tlyC gene in *Salmonella enterica* serovar *Typhimurium* mediates phagosomal escape. *Infect. Immun.* **73,** 6668–6673
7. Schaechter, M., Bozeman, F. M., and Smadel, J. E. (1957) Study on the growth of Rickettsiae. II. Morphologic observations of living Rickettsiae in tissue culture cells. *Virology* **3,** 160–172
8. Teysseire, N., Chiche-Portiche, C., and Raoult, D. (1992) Intracellular movements of *Rickettsia conorii* and *R. typhi* based on actin polymerization. *Res. Microbiol.* **143,** 821–829
9. Heinzen, R. A., Hayes, S. F., Peacock, M. G., and Hackstadt, T. (1993) Directional actin polymerization associated with spotted fever group *Rickettsia* infection of Vero cells. *Infect. Immun.* **61,** 1926–1935
10. Walker, D. H., Firth, W. T., and Edgell, C. J. (1982) Human endothelial cell culture plaques induced by *Rickettsia rickettsii*. *Infect. Immun.* **37,** 301–306
11. Sporn, L. A., Lawrence, S. O., Silverman, D. J., and Marder, V. J. (1993) E-selectin-dependent neutrophil adhesion to *Rickettsia rickettsii*-infected endothelial cells. *Blood* **81,** 2406–2412
12. Dignat-George, F., Teysseire, N., Mutin, M., Bardin, N., Lesaule, G., Raoult, D., and Sampol, J. (1997) *Rickettsia conorii* infection enhances vascular cell adhesion molecule-1- and intercellular adhesion molecule-1-dependent mononuclear cell adherence to endothelial cells. *J. Infect. Dis.* **175,** 1142–1152
13. Damås, J. K., Davi, G., Jensenius, M., Santilli, F., Otterdal, K., Ueland, T., Flo, T. H., Lien, E., Espevik, T., Frøland, S. S., Vitale, G., Raoult, D., and Aukrust, P. (2009) Relative chemokine and adhesion molecule expression in Mediterranean spotted fever and African tick bite fever. *J. Infect.* **58,** 68–75
14. Bechah, Y., Capo, C., Grau, G., Raoult, D., and Mege, J. L. (2009) *Rickettsia prowazekii* infection of endothelial cells increases leukocyte adhesion through $\alpha v\beta 3$ integrin engagement. *Clin. Microbiol. Infect.* **15,** 249–250
15. Clifton, D. R., Rydkina, E., Huyck, H., Pryhuber, G., Freeman, R. S., Silverman, D. J., and Sahni, S. K. (2005) Expression and secretion of chemotactic cytokines IL-8 and MCP-1 by human endothelial cells after *Rickettsia rickettsii* infection: regulation by nuclear transcription factor NF-κB. *Int. J. Med. Microbiol.* **295,** 267–278
16. Sporn, L. A., Haidaris, P. J., Shi, R. J., Nemerson, Y., Silverman, D. J., and Marder, V. J. (1994) *Rickettsia rickettsii* infection of cultured human endothelial cells induces tissue factor expression. *Blood* **83,** 1527–1534
17. Sporn, L. A., and Marder, V. J. (1996) Interleukin-1α production during *Rickettsia rickettsii* infection of cultured endothelial cells: potential role in autocrine cell stimulation. *Infect. Immun.* **64,** 1609–1613
18. Zhao, Y., Zhang, W., Kho, Y., and Zhao, Y. (2004) Proteomic analysis of integral plasma membrane proteins. *Anal. Chem.* **76,** 1817–1823
19. Bell, A. W., Ward, M. A., Blackstock, W. P., Freeman, H. N., Choudhary, J. S., Lewis, A. P., Chotai, D., Fazel, A., Gushue, J. N., Paiement, J., Palcy, S., Chevet, E., Lafrenière-Roula, M., Solari, R., Thomas, D. Y, Rowley, A., and Bergeron, J. J. (2001) Proteomics characterization of abundant Golgi membrane proteins. *J. Biol. Chem.* **276,** 5152–5165
20. Starkey, J. M., Zhao, Y., Sadygov, R. G., Haidacher, S. J., Lejeune, W. S., Dey, N., Luxon, B. A., Kane, M. A., Napoli, J. L., Denner, L., and Tilton, R. G. (2010) Altered retinoic acid metabolism in diabetic mouse kidney identified by O isotopic labeling and 2D mass spectrometry. *PLoS One* **5,** e11095
21. Sadygov, R. G., Zhao, Y., Haidacher, S. J., Starkey, J. M., Tilton, R. G., and Denner, L. (2010) Using power spectrum analysis to evaluate 18O-water labeling data acquired from low resolution mass spectrometers. *J. Proteome Res.* **9,** 4306–4312
22. Cox, J., and Mann, M. (2008) MaxQuant enables high peptide identification rates, individualized p.p.b.-range mass accuracies and proteome-wide protein quantification. *Nat. Biotechnol.* **26,** 1367–1372
23. Zybailov, B., Mosley, A. L., Sardiu, M. E., Coleman, M. K., Florens, L., and Washburn, M. P. (2006) Statistical analysis of membrane proteome expression changes in *Saccharomyces cerevisiae*. *J. Proteome Res.* **5,** 2339–2347
24. Zhao, Y., and Brasier, A. R. (2013) Applications of selected reaction monitoring (SRM)-mass spectrometry (MS) for quantitative measurement of signaling pathways. *Methods* **61,** 313–322
25. Zhao, Y., Tian, B., Edeh, C. B., and Brasier, A. R. (2013) Quantitation of the dynamic profiles of the innate immune response using multiplex selected reaction monitoring-mass spectrometry. *Mol. Cell. Proteomics* **12,** 1513–1529
26. Mi, H., Lazareva-Ulitsky, B., Loo, R., Kejariwal, A., Vandergriff, J., Rabkin, S., Guo, N., Muruganujan, A., Doremieux, O., Campbell, M. J., Kitano, H., and Thomas, P. D. (2005) The PANTHER database of protein families, subfamilies, functions and pathways. *Nucleic Acids Res.* **33,** D284–D288
27. Liu, H., Sadygov, R. G., and Yates, J. R., 3rd (2004) A model for random sampling and estimation of relative protein abundance in shotgun proteomics. *Anal. Chem.* **76,** 4193–4201
28. Old, W. M., Meyer-Arendt, K., Aveline-Wolf, L., Pierce, K. G., Mendoza, A., Sevinsky, J. R., Resing, K. A., and Ahn, N. G. (2005) Comparison of label-free methods for quantifying human proteins by shotgun proteomics. *Mol. Cell. Proteomics* **4,** 1487–1502
29. Paoletti, A. C., Parmely, T. J., Tomomori-Sato, C., Sato, S., Zhu, D., Conaway, R. C., Conaway, J. W., Florens, L., and Washburn, M. P. (2006) Quantitative proteomic analysis of distinct mammalian Mediator complexes using normalized spectral abundance factors. *Proc. Natl. Acad. Sci. U.S.A.* **103,** 18928–18933
30. Valbuena, G., and Walker, D. H. (2005) Changes in the adherens junctions of human endothelial cells infected with spotted fever group rickettsiae. *Virchows Arch.* **446,** 379–382
31. Santucci, L. A., Gutierrez, P. L., and Silverman, D. J. (1992) *Rickettsia rickettsii* induces superoxide radical and superoxide dismutase in human endothelial cells. *Infect. Immun.* **60,** 5113–5118
32. Kleba, B., Clark, T. R., Lutter, E. I., Ellison, D. W., and Hackstadt, T. (2010) Disruption of the *Rickettsia rickettsii* Sca2 autotransporter inhibits actin-based motility. *Infect. Immun.* **78,** 2240–2247
33. Jerrells, T. R., Li, H., and Walker, D. H. (1988) *In vivo* and *in vitro* role of γ interferon in immune clearance of *Rickettsia* species. *Adv. Exp. Med. Biol.* **239,** 193–200
34. Li, H., Jerrells, T. R., Spitalny, G. L., and Walker, D. H. (1987) γ interferon as a crucial host defense against *Rickettsia conorii in vivo*. *Infect. Immun.* **55,** 1252–1255
35. Colonne, P. M., Eremeeva, M. E., and Sahni, S. K. (2011) β interferon-mediated activation of signal transducer and activator of transcription protein 1 interferes with *Rickettsia conorii* replication in human endothelial cells. *Infect. Immun.* **79,** 3733–3743
36. Rydkina, E., Turpin, L. C., and Sahni, S. K. (2010) *Rickettsia rickettsii* infection of human macrovascular and microvascular endothelial cells reveals activation of both common and cell type-specific host response mechanisms. *Infect. Immun.* **78,** 2599–2606
37. Colonne, P. M., Sahni, A., and Sahni, S. K. (2013) Suppressor of cytokine signalling protein SOCS1 and UBP43 regulate the expression of type I interferon-stimulated genes in human microvascular endothelial cells infected with *Rickettsia conorii*. *J. Med. Microbiol.* **62,** 968–979
38. George, F., Brouqui, P., Boffa, M. C., Mutin, M., Drancourt, M., Brisson, C., Raoult, D., and Sampol, J. (1993) Demonstration of *Rickettsia conorii*-induced endothelial injury *in vivo* by measuring circulating endothelial cells, thrombomodulin, and von Willebrand factor in patients with Mediterranean spotted fever. *Blood* **82,** 2109–2116
39. Feng, H., Popov, V. L., Yuoh, G., and Walker, D. H. (1997) Role of T lymphocyte subsets in immunity to spotted fever group rickettsiae. *J. Immunol.* **158,** 5314–5320
40. Walker, D. H., Olano, J. P., and Feng, H. M. (2001) Critical role of cytotoxic T lymphocytes in immune clearance of rickettsial infection. *Infect. Immun.* **69,** 1841–1846
41. Li, Z., Díaz-Montero, C. M., Valbuena, G., Yu, X.-J., Olano, J. P., Feng, H.-M., and Walker, D. H. (2003) Identification of CD8 T-lymphocyte epitopes in OmpB of *Rickettsia conorii*. *Infect. Immun.* **71,** 3920–3926
42. Sporn, L. A., Shi, R. J., Lawrence, S. O., Silverman, D. J., and Marder, V. J. (1991) *Rickettsia rickettsii* infection of cultured endothelial cells induces release of large von Willebrand factor multimers from Weibel-Palade bodies. *Blood* **78,** 2595–2602
43. Kulig, P., Kantyka, T., Zabel, B. A., Banas, M., Chyra, A., Stefanska, A., Tu, H., Allen, S. J., Handel, T. M., Kozik, A., Potempa, J., Butcher, E. C., and Cichy, J. (2011) Regulation of chemerin chemoattractant and antibacterial activity by human cysteine cathepsins. *J. Immunol.* **187,** 1403–1410
44. Sahni, S. K., Kiriakidi, S., Colonne, M. P., Sahni, A., and Silverman, D. J. (2009) Selective activation of signal transducer and activator of transcription (STAT) proteins STAT1 and STAT3 in human endothelial cells infected with *Rickettsia rickettsii*. *Clin. Microbiol. Infect.* **15,** 303–304